doi:10.1093/brain/awx374 BRAIN 2018: 141; 713–730 | 713

BRAIN
A JOURNAL OF NEUROLOGY

Stereotyped high-frequency oscillations discriminate seizure onset zones and critical functional cortex in focal epilepsy

Su Liu,[1] Candan Gurses,[2] Zhiyi Sha,[3] Michael M. Quach,[4] Altay Sencer,[5] Nerses Bebek,[2] Daniel J. Curry,[6] Sujit Prabhu,[7] Sudhakar Tummala,[7] Thomas R. Henry[3] and Nuri F. Ince[1]

High-frequency oscillations in local field potentials recorded with intracranial EEG are putative biomarkers of seizure onset zones in epileptic brain. However, localized 80–500 Hz oscillations can also be recorded from normal and non-epileptic cerebral structures. When defined only by rate or frequency, physiological high-frequency oscillations are indistinguishable from pathological ones, which limit their application in epilepsy presurgical planning. We hypothesized that pathological high-frequency oscillations occur in a repetitive fashion with a similar waveform morphology that specifically indicates seizure onset zones. We investigated the waveform patterns of automatically detected high-frequency oscillations in 13 epilepsy patients and five control subjects, with an average of 73 subdural and intracerebral electrodes recorded per patient. The repetitive oscillatory waveforms were identified by using a pipeline of unsupervised machine learning techniques and were then correlated with independently clinician-defined seizure onset zones. Consistently in all patients, the stereotypical high-frequency oscillations with the highest degree of waveform similarity were localized within the seizure onset zones only, whereas the channels generating high-frequency oscillations embedded in random waveforms were found in the functional regions independent from the epileptogenic locations. The repetitive waveform pattern was more evident in fast ripples compared to ripples, suggesting a potential association between waveform repetition and the underlying pathological network. Our findings provided a new tool for the interpretation of pathological high-frequency oscillations that can be efficiently applied to distinguish seizure onset zones from functionally important sites, which is a critical step towards the translation of these signature events into valid clinical biomarkers.

1 Department of Biomedical Engineering, University of Houston, Houston, Texas, USA
2 Department of Neurology, Istanbul Faculty of Medicine, Istanbul University, Istanbul, Turkey
3 Department of Neurology, University of Minnesota, Minneapolis, Minnesota, USA
4 Department of Neurology, Texas Children's Hospital, Baylor College of Medicine, Houston, Texas, USA
5 Department of Neurosurgery, Istanbul Faculty of Medicine, Istanbul University, Istanbul, Turkey, USA
6 Department of Neurosurgery, Texas Children's Hospital, Baylor College of Medicine, Houston, Texas, USA
7 Department of Neurosurgery, MD Anderson Cancer Center, University of Texas, Houston, Texas, USA

Correspondence to: Nuri F. Ince, PhD
Department of Biomedical Engineering
University of Houston
HBS Building 592, Rm 334
4849 Calhoun Rd.
Houston, TX 77204, USA
E-mail: nfince@uh.edu

Received May 31, 2017. Revised October 8, 2017. Accepted November 12, 2017. Advance Access publication January 30, 2018

Keywords: epilepsy; high-frequency oscillations; seizure onset zone; intracranial EEG

Abbreviations: DCS = direct cortical mapping; f/o/sHFO = HFOs inside the functional area/inside the SOZ/outside the SOZ; HFO = high-frequency oscillation; iEEG = intracranial EEG; SOZ = seizure onset zone

Introduction

Resective epilepsy surgery can fully control seizures in selected patients with seizures that are refractory to medications (Engel *et al.*, 2003; de Tisi *et al.*, 2011). Surgical removal of the seizure onset zone (SOZ) often requires electrophysiological recordings of habitual seizures using intracerebral ('depth') and subdural macroelectrodes, placed in hypothesized candidate sites of seizure onset (So *et al.*, 1989; Engel *et al.*, 1990; Henry *et al.*, 1999; Brna *et al.*, 2015). Accurate detection of an epileptogenic zone is generally accomplished through intracranial electroencephalographic (iEEG) monitoring over an extended period of time and detailed visual inspection of these local field potential data by medical experts. High frequency oscillations (HFOs, 80–500 Hz) recorded in iEEG have been proposed as promising neuro-biomarkers for epileptogenic tissue. Studies over the last decade have shown that HFO transients are significantly correlated with ictogenesis (Allen *et al.*, 1992; Jirsch *et al.*, 2006; Urrestarazu *et al.*, 2006; Zijlmans *et al.*, 2011). Despite the potential benefits, it is still challenging to introduce HFO results in clinical practice. Multiple reports indicate that HFOs can be generated not only by epileptic cerebral tissue but also by non-epileptic sites often including motor cortex, visual cortex and language areas (Sinai *et al.*, 2005; Nagasawa *et al.*, 2012; Matsumoto *et al.*, 2013; Kucewicz *et al.*, 2014). The co-occurrence of pathological HFOs and physiological HFOs may interfere with the delineation of ictogenesis and increase the risk of injury to functional areas, as the spatial distribution of physiological HFOs can correlate with brain regions that are not responsible for seizure generation but functionally important and need to be preserved during resection.

Discrimination between physiological and pathological HFOs is incompletely understood at present. Spectral frequency alone is not a reliable differential feature (Bragin *et al.*, 2007; Köhling and Staley, 2011), as pathological HFOs may contain significant spectral power in the ripple-band (80–200 Hz) (Traub *et al.*, 2001), which had been historically linked to physiological activities (reviewed in Zijlmans *et al.*, 2012). Further, fast ripples (200–500 Hz) have been observed in normal brain structures associated with visual perception, which also complicates the clinical use of HFOs as valid biomarkers to guide epilepsy surgery (Jacobs *et al.*, 2008; Dümpelmann *et al.*, 2012; Kerber *et al.*, 2014). Several recent studies investigated differences between HFOs discovered inside and outside the SOZ (Melani *et al.*, 2013; Kerber *et al.*, 2014); others compared pathological HFOs with oscillations induced by motor/visual tasks or cortical stimulation (Matsumoto *et al.*, 2013; Nonoda *et al.*, 2016). The investigators generally performed visual marking of HFOs in a predefined subset of data, then looked into features related to the rate of HFO occurrence, amplitude, duration, frequency, and their interaction with slow waves or baseline activities; some also attempted to differentiate between epileptic and non-epileptic HFOs using supervised classifiers based on the abovementioned features (Nagasawa *et al.*, 2012; Alkawadri *et al.*, 2014; Burnos *et al.*, 2016; von Ellenrieder *et al.*, 2016). Although some of the features presented group-wise statistical difference, these features poorly discriminate epileptic and non-epileptic HFOs in individual subjects and so cannot yet be used to improve clinical decision-making.

In our prior study, we proposed an automated HFO detector based on clustering the time-frequency features of candidate events for the quantitative process of massive iEEG data produced by continuous recordings (Liu *et al.*, 2016). Based on initial visual inspection within the identified HFO clusters we observed that HFOs generated from seizure onset zones tended to be similar in wave shape, and repetitively occur throughout the recording, compared with greater qualitative variability of HFOs in other sites. We hypothesized that pathological HFOs occur in a repetitive fashion with a similar waveform morphology that specifically indicate seizure onset zones. Here we expanded our previous method and by using a pipeline of unsupervised machine learning techniques we captured a new pattern of HFOs with highly stereotyped waveforms in large iEEG recordings automatically. We investigated these 'clones' of HFO waveforms in 13 patients with focal epilepsy and five control patients with brain tumour but no epilepsy, where subdural electrocorticogram (ECoG) grids are implanted for the mapping of the eloquent brain regions. In particular, we aimed to clarify whether the recurrence of similar HFO waveforms is exclusively linked to seizure focus, such that it can be used to facilitate the discrimination between SOZ and other functional regions.

Material and methods

Patient population

Eighteen subjects were included in the study (12 females), including 13 patients with intractable temporal lobe or extratemporal neocortical epilepsy (Patients 1–13), and five control subjects with brain tumour but no epilepsy who went through intraoperative functional mapping in an awake surgery (Controls 1–5). The inclusion criteria for epilepsy cohort consisted of the following: patients

with intractable temporal lobe or extratemporal lobe epilepsy who went through iEEG monitoring with video after the implantation of subdural grid or depth electrodes in University of Minnesota (UMN, Minneapolis, Minnesota), Istanbul Faculty of Medicine at Istanbul University (IU, Istanbul, Turkey), and Texas Children's Hospital (TCH, Houston, Texas). This yielded a total of 13 patients, including 10 adults (aged 30–53 years) and three paediatric patients (aged 3–18 years). Additional data were collected using the same recording system at Istanbul University and MD Anderson Cancer Center (MDA, Houston, Texas) from five control subjects with brain tumour but no epilepsy history who underwent intraoperative cortical stimulation to identify the functional cortex. These subjects were involved for the investigation of non-epileptic HFOs originating from functional regions. Data collection and scientific workup were approved by the Institutional Review Board of each institution.

Electrode placement and intracranial EEG recording

In the 13 patients with epilepsy, a combination of surface and depth electrodes were implanted to the possible irritative sites for the accurate delineation of the SOZ. Subdural grid arrays were placed over the functional region in 10 subjects to give a sufficient coverage of the eloquent cortex (Patients 9–13 and Controls 1–5). Post-implantation MRI/CT or intraoperative photos were taken to determine the electrode locations in all subjects.

Multichannel iEEG data were obtained with 2 kHz (at UMN) or 2.4 kHz (at IU, TCH and MDA) sampling frequency and 24 bit A/D resolution using g.HIamp system (g.tec Medical Engineering) with an anti-aliasing filter set to 600 Hz. For Patients 1–13, continuous iEEG signal was recorded for 2–4 days in the EMU simultaneously with video monitoring throughout the period. For Controls 1–5, data were recorded intraoperatively in the awake state for 40–50 min. In four of our control patients (Controls 2–5), ECoG electrode grids with more than 100 contacts (4-mm centre to centre spacing) were used to cover peri-tumour area and to map the functional regions. In these control subjects, we recorded extended length of baseline/resting period (10–15 min) followed by 30–35 min of functional tasks in the operating room, where the subject stayed awake during the entire recording and executed a functional task such as hand/arm movements or responded to an external stimulus such as touching hands/fingers. Then a direct cortical stimulation (DCS) procedure was executed to find functional cortical areas.

Delineation of the seizure onset zone and functional regions

For the epilepsy cohort, the seizure onset channels with earliest ictal discharges were visually determined by neurologists based on the long-term video iEEG monitoring. In 10 subjects, functional regions were defined by cortical mapping, which was performed as a part of the clinical routine, including five patients with epilepsy where the implanted grid electrodes covered the motor/language areas, and five control subjects without history of epilepsy. Specifically, the functional areas included motor cortex (Patients 9, 12, and 13; Controls 1, 2, 4, and 5), somatosensory cortex (Patients 11, 12, and Control 3), and Broca's area (Patient 10). DCS was conducted between pair of contacts with a current amplitude ranging from 1 to 15 mA, pulse width of 200–300 μs, and duration of 0.2 s, according to the patient's individual tolerance.

Data selection and high frequency oscillation detection

All data were de-identified and transferred to University of Houston for the offline analysis in MATLAB environment (Mathworks, MA, USA). For Patients 1–13 who underwent prolonged recording in the EMU, 60 min of continuous iEEG data in the waking baseline (at least 4 h away from the first seizure) was used per patient according to the clinical annotations to obtain a sufficient number of HFO events. For Controls 1–5, the entire intraoperative recording was used for the analysis.

Detection of HFOs and their waveform patterns was performed by using a pipeline of unsupervised machine learning techniques, which is provided in Fig. 1. HFOs were automatically identified in all recorded channels using a previously published detector (Liu *et al.*, 2016) with modifications. In brief, raw iEEG data firstly went through an amplitude-based detector after band-pass filtering within the 80–500 Hz range. Short-time Fourier transform (STFT) was then performed on the original raw signal in each remaining candidate, followed by a denoising step to eliminate minor background activities on the time-frequency map. The denoising level, detection threshold and other parameters were consistent with our previous studies (Liu *et al.*, 2015, 2016). For all surviving events, the entire iEEG bandwidth was explored, where three time-frequency features (sub-band power ratio, entropy of the spectrum, and frequency corresponding to maximum peak-to-notch ratio) were extracted and used with Gaussian Mixture Model clustering with *k-medoids* initialization (Kaufman and Rousseeuw, 2002) to isolate HFOs from spikes and other arbitrary events. The sub-band power ratio after denoising the time frequency plane served as a useful feature to distinguish spikes from HFOs, as HFOs had an isolated component above 80 Hz after denoising but not the spikes. The entropy was used to assess the sharpness of the spectrum, which helped to isolate HFOs from sharp waves or white noise with uniform energy in the spectrum. Finally, the frequency corresponding to maximum peak to notch ratio served as a useful feature to separate subtypes of HFOs with distinct frequency components above 80 Hz.

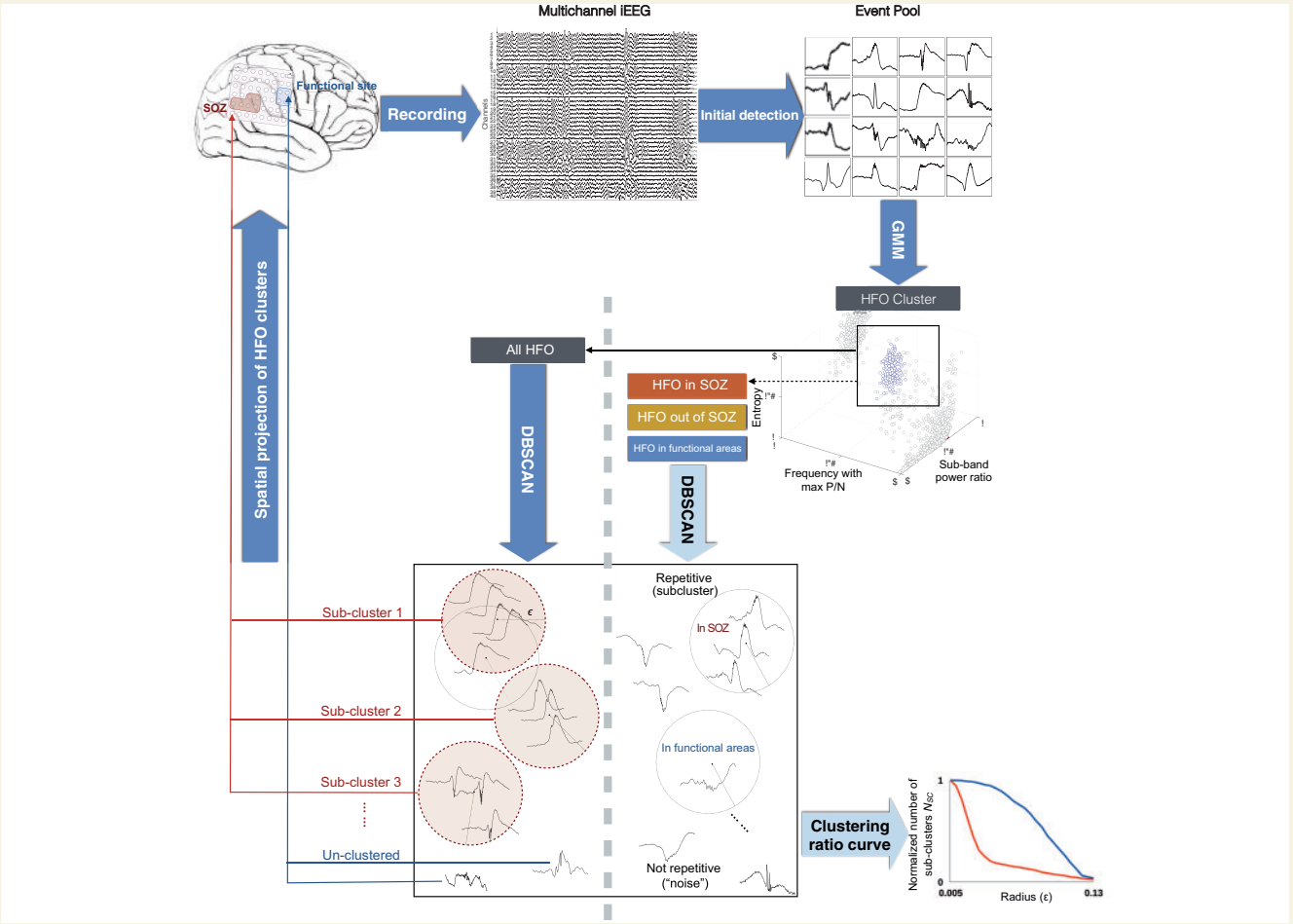

Figure 1 Data analysis workflow. After initial amplitude-based detection, HFOs were isolated from other events by using a clustering-based approach with time-frequency features. The resulting HFO clusters were then categorized by their spatial origins for a group-wise comparison of the repetitive pattern after computing the clustering ratio curves (*bottom right*). Finally, the stereotyped HFO patterns were blindly projected to the brain, the spatial distribution was correlated with the clinician-defined SOZ and functional regions.

The cluster number was determined based on the elbow method (Ketchen and Shook, 1996).

After generating a pool of HFOs, we categorized them according to their spatial origin and group comparison was performed among HFOs inside the SOZ (sHFO), outside the SOZ (oHFO), and inside the functional areas (fHFO) across patients. Classic HFO features including mean frequency and rate of occurrence were also inspected. The detection of recurrent HFO subclusters within sHFO, oHFO and fHFO was implemented using the procedures described in the section below.

Detection of stereotyped high frequency oscillations

Following a visual inspection of HFOs in a few subjects, we observed that HFOs originated from epileptic tissues tended to occur repeatedly with similar waveform morphology, raising a presumption that pathological HFOs might produce compact subclusters in the high-dimensional native space, with each of the subcluster being a group of events that shared the same waveform pattern. In comparison, HFO members detected in non-SOZ areas were assumed to present irregular wave shapes with relatively large intra-cluster distance in native space. To uncover this underlying pattern in an objective and unbiased manner, we performed the detection using the density-based spatial clustering of applications with noise (DBSCAN) approach (Ester *et al.*, 1996). The original algorithm was designed to identify dense regions in a dataset by grouping data points neighbouring a 'core point' within a certain radius 'epsilon' (ε). The radius also represents the distance between two events (measure of dissimilarity). The 'core point' is defined as a point with its neighbour count exceeding a user-specified threshold *MinPts*. After isolating the HFO events with the Gaussian Mixture Model method, we executed DBSCAN algorithm to capture subclusters of stereotyped HFO waveforms. Specifically, we implemented the algorithm in different HFO groups (sHFO, oHFO and fHFO) with an increasing sequence of ε, computed the

corresponding number of subcluster (N_{SC}), and visualized the estimation result by plotting the curves of clustering ratio (N_{SC} versus ε), which is the change in the number of detected subclusters within each HFO group for different distance values. The initial ε was assigned to 0, with *MinPts* of 1, such that each HFO event in the group was taken as an individual subcluster at the first place. Given that closely spaced points would be merged instantly as the cluster radius ε expanded, we expected to observe an immediate drop in the N_{SC} value in sHFO datasets with repetitive waveform patterns (Fig. 1). Thus, the difference in waveform patterns among sHFO, oHFO and fHFO groups can be quantified by comparing the area under curve (AUC) between groups. The estimation was executed in HFO data after removing the low-band component below 4 Hz. The dissimilarity between pairs of the signals was computed using Euclidean distance. Before computing the distance between two HFO events, they are aligned with each other using the index corresponding to the maximum absolute cross-correlation. Specifically, we calculated the cross-correlation function for different lags (±10 ms) of two signals and used the lag that provided maximum absolute cross-correlation value to minimize the influence of phase shift between two similar events during distance calculation.

Identification of seizure onset zone using stereotyped high frequency oscillations

In this stage, we investigated if stereotyped HFO waveform patterns could be used in the discrimination of SOZ and eloquent areas in a blinded fashion. This was done by executing DBSCAN in all HFOs recorded from each patient without grouping them according to their origins, and quantifying the change in spatial distribution of HFOs when the degree of signal dissimilarity increased.

After using the Gaussian Mixture Model clustering in 3D feature space on the entire candidate event population and forming the HFO pool, we identified repetitive HFO waveforms in Patients 1–11, using an increasing value of ε from 0.05 to 1 and a fixed *MinPts* of 3. At each ε level, the algorithm discovered subclusters of stereotypical HFO waveforms with intra-cluster distance smaller than the current ε. We computed the proportion of clustered HFOs inside the SOZ, inspected the spatial distribution of HFOs with and without a repetitive waveform pattern, and discussed their correlation with SOZ and functional regions. For each patient, the spatial maps of HFOs were projected to a 3D model of the brain, which was generated after the coregistration of post-implantation CT image and the individual's MRI. Finally, we sought to clarify whether the highly correlated HFOs (i.e. clustered by DBSCAN using a small radius) give specific information about the SOZ, and evaluated the predictive performance when these HFOs were used for SOZ localization. More precisely, we determined the number of channels with repetitive HFO patterns (CH_R) and without a repetitive pattern (CH_{NoR}), and then evaluated their relationship with SOZ channels by calculating the sensitivity, specificity and accuracy (Burnos *et al.*, 2014), which were defined as:

$$\text{Sensitivity} = \frac{CH_R \text{ in SOZ}}{CH_R \text{ in SOZ} + CH_{NoR} \text{ in SOZ}} \quad (1)$$

$$\text{Specificity} = \frac{CH_{NoR} \text{ not in SOZ}}{CH_{NoR} \text{ not in SOZ} + CH_R \text{ not in SOZ}} \quad (2)$$

$$\text{Accuracy} = \frac{CH_R \text{ in SOZ} + CH_{NoR} \text{ not in SOZ}}{\text{Number of total Channels}} \quad (3)$$

Statistical analysis

We compared the HFO rates, mean frequency, the minimum clustering radius and area under the clustering ratio curve inside and outside the SOZ using a two-tailed non-parametric Wilcoxon signed rank test with a confidence interval (CI) of 95%. A Wilcoxon rank sum test was carried out to compare the signal characteristics between fHFO and the other two groups across patients. The same test was also applied for the comparison between epilepsy and control cohorts.

Results

Seizure onset zone identification and functional mapping results

Demographic and clinical information for all subjects is provided in Supplementary Table 1. In each individual subject 28–120 channels were implanted and recorded by the system. SOZ was visually identified by neurologists in 11 patients (Patients 1–11) after electrode placement and the following long-term video EEG monitoring. In each patient, 2–14 channels where the earliest clear electroencephalographic discharges started were determined by the neurologists and marked as the SOZ. As a result, 92 of 1309 channels were defined as the SOZ, accounting for 15% of the channels in Patients 1–11, and 7% of the total recorded channels. Surgical resection was tailored based on the SOZ delineation on an individual basis. After 12–24 months of follow-up, at the time of writing (May 2017) all patients received significant seizure reduction with Engel class I or II outcome (Engel, 1987). In two patients (Patients 12 and 13) the SOZ could not be identified after initial implantation. In these cases the grid electrodes covered eloquent areas of the brain, and the data were used for functional HFO analysis only. Two patients (Patients 2 and 8) were not treated with resective epilepsy surgery. Patient 8 was implanted with an RNS device, which provided 80% reduction in seizures. In Patient 2, SOZ was

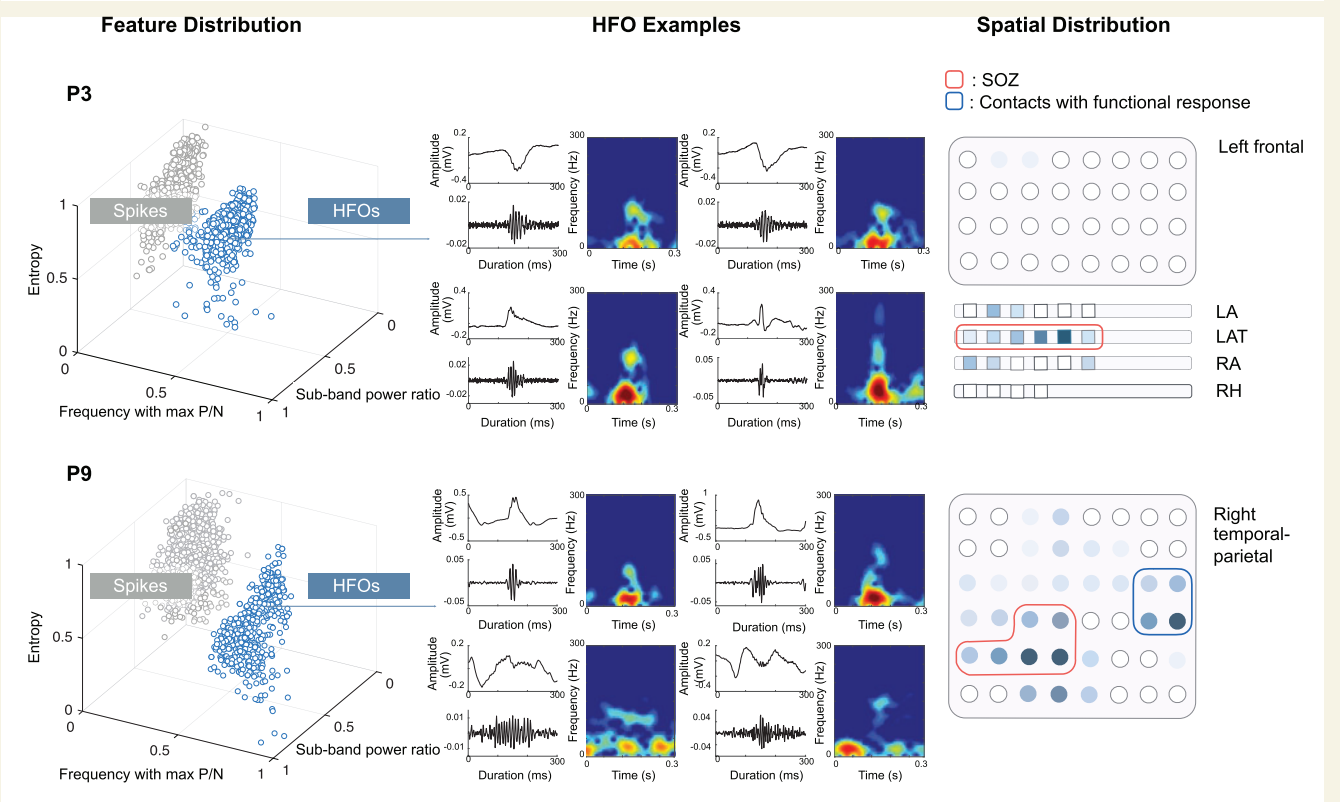

Figure 2 Three-dimensional distribution of HFO and spikes identified by Gaussian Mixture Model clustering in two patients. HFOs clusters are marked in blue. For each patient, four random HFO samples from the cluster are displayed with raw data, the high-pass filtered signal (>80 Hz) and the time-frequency maps showing the high frequency components above 80 Hz. The spatial distribution of the identified HFO cluster is given on the electrode sketch in the last column. Higher HFO rate is represented by darker shades. In Patient 9 (P9), the HFOs were generated from both the SOZ (marked by red line) and functional area identified by DCS mapping (marked by blue line). LA = left anterior; LAT = left anterior temporal; RA = right amygdala; RH = right hippocampus; P/N = peak to notch ratio; P3 = Patient 3.

defined through prolonged EMU monitoring, and the patient became seizure-free persistently following the removal of intracranial depth electrodes. Patient 2 did not have any new lesion that was detected with MRI following electrode removal. The phenomenon of prolonged remission of intractable partial epilepsy following implantation of intracranial electrodes is rarely encountered, but has been established as a definite clinical syndrome (Katariwala *et al.*, 2001). The pathophysiological basis of this phenomenon is not entirely known; some evidence suggests that small cerebral injuries incurred by electrode implantation may permanently alter ictal initiation or propagation sites, even though postoperative brain MRI may not detect new iatrogenic lesions, which can be quite small.

DCS was performed in five patients with epilepsy (Patients 9–13) and all control subjects (Controls 1–5) intraoperatively to map the eloquent cortex. Functional responses were detected in primary motor cortex (Patients 9, 12, 13, and Controls 1, 2, 4 and 5), somatosensory cortex (Patients 11 and 12, and Control 3), and Broca's area (Patient 10). The total number of channels with functional response was 138, accounting for 11% of the recorded channels, with 2–34 contacts being identified per subject.

Unsupervised high frequency oscillation detection

Across 16 subjects, 28 832 events were captured in the 16.5 h of recording during the amplitude-based detection stage, generating the initial pool of candidates. In each patient, the events in the candidate pool were categorized into two to four clusters in 3D feature space using the Gaussian Mixture Model method, which generally consisted of one or two clusters of HFOs, with other clusters being mixtures of irregular waveforms or artefacts. In the epilepsy group, one additional cluster of spikes was identified consistently per patient. This step helped us to successfully isolate HFOs from spikes and other events. The scatter plots of two representative patients (Patients 3 and 9) showing the distribution of detected events in 3D feature space are given in Fig. 2. For each HFO cluster, four random event members and their filtered signal above 80 Hz are displayed together with the time-frequency maps, to give a flavour of the cluster content. For each patient, the spatial extent of HFO cluster is presented on the electrode sketch in the last column. Although the majority of the HFOs are located in the SOZ in Patient 3, the large portion of HFOs recorded

from the functional area in Patient 9 evidences that HFO rate alone will not be sufficient to identify the SOZ in certain cases.

Comparison of high frequency oscillations originating from different locations

In total, 13 011 HFOs were isolated by the unsupervised detection based on the Gaussian Mixture Model and were investigated in the subsequent analysis. The number of HFO-generating channels in each patient ranged from 9 to 77. In epilepsy patients with clear SOZ definition (Patients 1–11), HFOs were found in 60% of the channels. In Patients 12 and 13 and Controls 1–5, where the electrode covered the functional cortex only, the HFOs were located in 38% of the recorded channels. Based on the SOZ delineation and functional mapping results, the HFO candidates were first grouped according to their spatial locations. Overall, 41% of HFOs were detected from the seizure onset channels in Patients 1–11 and were named as 'sHFO'. In these same patients, 32% of HFOs were detected from other brain regions excluding the SOZ and functional regions. These HFOs were denoted as 'oHFO'. Finally, 19% of the HFOs were recorded from the functional regions such as the motor or language cortex in 10 subjects, where functional mapping was performed, and hence were labelled as 'fHFO'. The remaining 8% of the HFOs originated from cortical regions out of the functional locations identified by the direct cortical stimulation in control subjects, and were excluded from the analysis to maintain consistency.

In Fig. 3 we provide boxplots showing the comparison among sHFO, oHFO and fHFO groups in terms of mean frequency and the rate of occurrence in each individual patient with SOZ definition. In all patients, the HFO frequency ranges were largely overlapped. Although for many patients the rates of sHFO and oHFO were clearly distinct, in Patients 6 and 7 the channel with the highest HFO rate did not correspond to the SOZ; in Patient 9 the channel over the functional area had HFO rates larger than the SOZ. Overall, the sHFO events possessed higher mean frequency compared to the other two HFO types (sHFO = 154 Hz, oHFO = 146 Hz, fHFO = 150 Hz, $P < 10^{-3}$), with substantial overlaps across groups. The average rate per channel for sHFO = 1.2/min, which was significantly higher than oHFO (0.2/min, $P < 10^{-3}$) but comparable to fHFO events (1.0/min, $P = 0.4$). The rate of fHFO was also significantly higher compared to oHFO ($P < 0.01$).

Stereotyped high frequency oscilaltion waveform patterns

We executed DBSCAN clustering in sHFO, oHFO and fHFO groups in each patient to identify subclusters of repetitive HFOs with similar morphometric waveform patterns, without prior knowledge on the shape of the raw signal. Highly stereotyped HFO waveforms in varying shapes were observed from single or multiple sources in individual patients. In Fig. 4A we present examples of repetitive HFO waveform subclusters and HFOs without a repetitive pattern in five patients, where the seizures started from hippocampal structures (in Patients 1 and 2), neocortical temporal lobe (in Patient 3), parietal lobe (in Patient 9) and frontal lobe (in Patient 10), respectively. For each type of HFO, four individual samples and the pile plot of events in the same subcluster are shown, along with the averaged time-frequency map. The origin of the presented HFOs are marked on the electrode contacts in red if it's inside the SOZ, yellow if it's outside the SOZ, or blue if it's located inside the functional area. As shown in Fig. 4A, in each patient the HFOs commonly associated with repetitive waveform patterns in the form of slow waves, spikes or sharp waves resigning in the low band. These repetitive waveforms with HFOs were recorded from a subset of SOZ channels, which was distinct from the unclustered HFOs appearing more frequently with oscillating background activities and not correlated with the SOZ.

To give more insight into these stereotypical waveform structures, we visualized the distance matrix of HFOs by plotting a circular network for each HFO group. In Fig. 4B, we first provide the results obtained from 13 HFO samples, which were manually selected based on their waveform morphology. In the network, each node represents a HFO observation, which is connected to other samples by edges in different shades indicating the strength of the relevant connection. In our case, a strong connection provides smaller Euclidean distance demonstrating higher similarity between two HFO candidates. HFOs with very similar waveforms provide linkage in darker shades. The connectivity of subsets of events in one representative patient (Patient 9) is shown in Fig. 4C, where HFOs were detected inside the SOZ, out of the SOZ, and from the functional sites of this patient, respectively. The result suggested a much stronger correlation between events in the sHFO group compared to oHFO and fHFO groups. The 'gap' in the network graph indicates that at least two distinct patterns exist among the presented sHFO candidates, each of which shared compact intra-subgroup connectivity but barely correlated with the other pattern. Quite weak connectivity was observed in the fHFO network compared to the other two groups. These results suggested that with different distance thresholds SOZ could be distinguished from functional and other regions by investigating the HFO waveform similarity between the captured events.

Figure 5A displays the curve of clustering ratio (N_{SC} versus ε) for three representative patients. The number of subclusters (N_{SC}) is normalized to the total number of events in each HFO group. For a distance $\varepsilon = 0$, where the constraint is to have identical waveforms, the number of subclusters is equal to the number of events. As the ε or the radius of possible subclusters increased, the N_{SC} values started to decrease for all groups but dramatically faster for sHFO events, where we consistently observed subclusters of

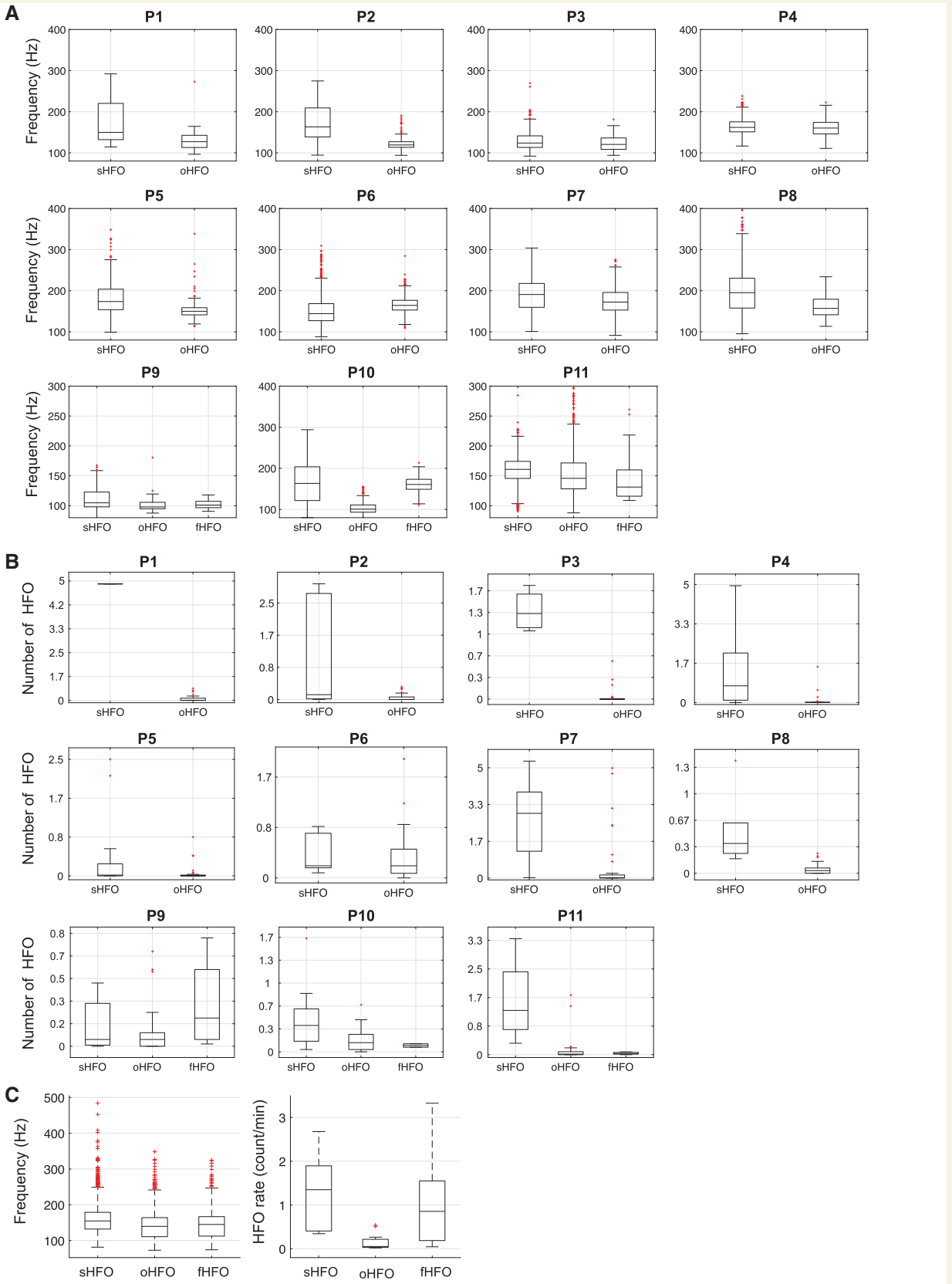

Figure 3 Frequency and rate of sHFO, oHFO and fHFO events. (**A**) Mean frequency of sHFO, oHFO (in Patients 1–11) and fHFO (in Patients 9–11) for each individual patient. (**B**) Number of sHFO, oHFO (in Patients 1–11) and fHFO (in Patients 9–11) for each individual patient. (**C**) Group comparison results across all subjects indicate that the mean frequency for sHFO is higher than oHFO and fHFO events, however the results suggested substantial overlaps exist across groups. The highest occurrence rate is observed in sHFO group. The difference is significant compared to oHFO but not to fHFO events.

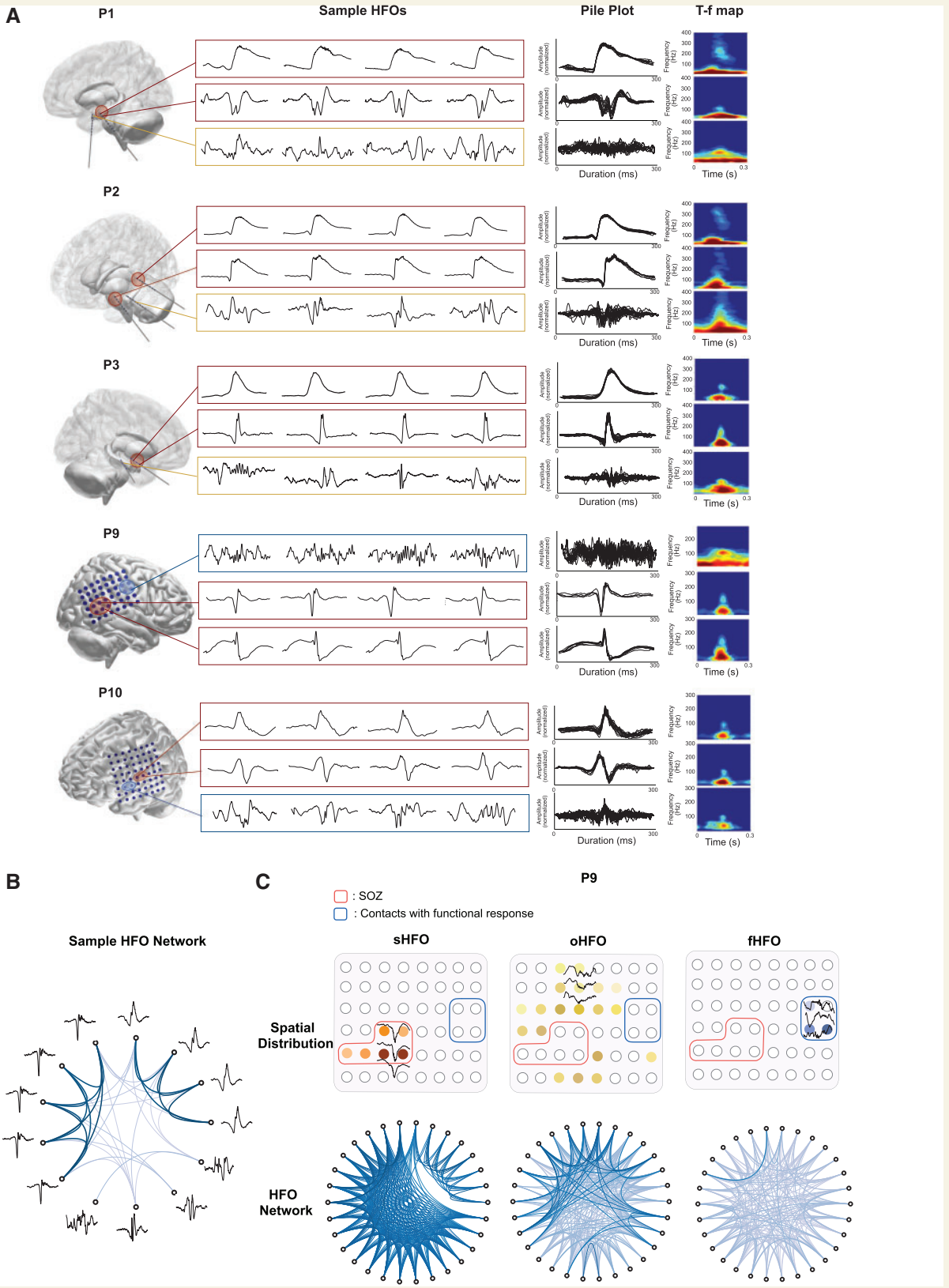

Figure 4 Stereotyped HFOs and HFOs without any repetitive pattern. (**A**) Examples of HFO subclusters and their spatial locations in five patients. For each HFO group, the pile plots and averaged time-frequency (T-f) map are provided (up to 20 events are shown), the spatial origins are marked on electrode contacts. In Patient 1, repetitive HFOs in different forms were generated by epileptic hippocampal structure. In Patient 2, repetitive HFOs were generated by posterior hippocampus and amygdala, both of which appeared to be epileptogenic. In Patient 3, highly similar ripples were found in the temporal lobe. In these patients, HFOs without a repetitive pattern are commonly observed in brain

(continued)

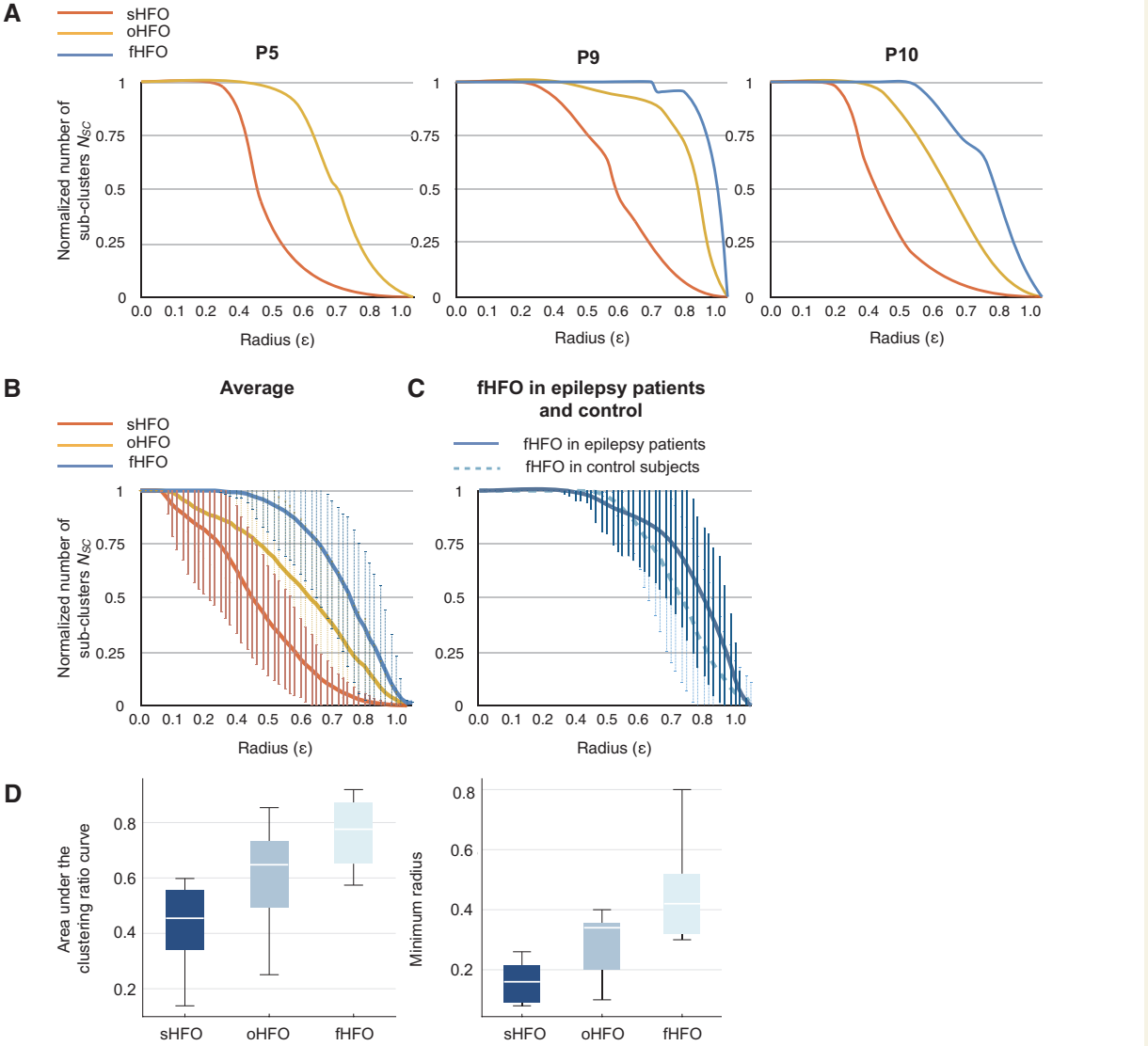

Figure 5 Characterization of clustering ratios in sHFO, oHFO, and fHFO. (**A**) Clustering ratio curves for three representative patients showing the change in number of subclusters (*Nsc*) with respect to the cluster radius (ε). The results indicate a compact and inhomogeneous distribution of sHFO events. (**B**) The average clustering ratio plots demonstrate the difference in HFO waveform patterns among sHFO, oHFO and fHFO groups. The most 'repetitive' patterns, as illustrated by a sharper decline in the curves, are observed in the sHFO group. (**C**) The curves in fHFOs of epilepsy patients and controls show similar characteristics. (**D**) Boxplots showing group differences in the AUC of clustering ratio curves and minimum ε to generate subclusters. These two features related to the waveform pattern showed little overlap between sHFO and fHFO groups.

recurrent HFO waveforms for moderate distance values ($\varepsilon < 0.5$).

The averaged plots in Fig. 5B were computed from sHFO and oHFO groups in 11 patients, and fHFOs in 10 subjects with functional mapping. We noted that, in all cases the N_{SC} values for sHFO exhibited a sharper decline as soon as the cluster radius reached a relatively small value (≈0.1). For oHFO and fHFO groups, by contrast, the initial ε

Figure 4 Continued
regions out of the SOZ. In Patients 9 and P10, while recurrent HFO patterns were seen in the SOZ (temporo-parietal and frontal region), the irregular HFOs were mostly seen in the functional motor cortex. (**B**) Circular network visualizing the distance matrix in 13 HFO samples. HFOs (nodes) are connected by edges that indicate the Euclidean distance (dissimilarity) between two events. While highly correlated similar HFOs provide linkage in dark shades, HFOs in distinct shapes provide weak or invisible connections. (**D**) Circular networks in three groups of HFOs, each being composed of 30 events recorded inside the SOZ, out of the SOZ, and inside the motor area in Patient 9. The compact connectivity and the blank space in between suggest the existence of two distinct patterns in the sHFO group. The connectivity is weakest in the fHFO groups compared to the other two suggesting the non-repetitive nature of fHFOs.

where individual observations started to merge were significantly larger, as with the AUC ($P < 0.01$) (Fig. 5D). The difference was more evident between sHFO and fHFO groups ($P < 10^{-3}$). The initial 'plateau' in the curves of fHFO group implied a relatively large and uniform spacing of the members, which then gradually fell to the bottom. The comparison of initial clustering radius ε between oHFO and fHFO also showed significant difference ($P < 0.05$), suggesting that fHFO events may exhibit greater variability in signal shapes. These results indicate that SOZ tend to produce stereotypical HFOs with quite repetitive waveform morphology whereas the HFOs occurring in functional areas are relatively irregular in their wave shapes.

Comparison of high frequency oscillations in epilepsy patients and the control group

We sought to determine whether the functional HFOs recorded from controls also followed the same irregular waveform characteristic with those recorded from patients with epilepsy. A total of 3207 HFOs were recorded from the five control subjects and 73% of these HFOs were detected from the contact locations identified by DCS, whereas the remaining 27% of events were located at the surrounding cortical regions. The fHFOs recorded in control subjects were compared with the sHFOs in 11 epilepsy patients, as well as the other fHFOs recorded from the motor/language areas of the five epilepsy patients. Figure 5C demonstrates the clustering ratio curves of fHFO in epilepsy and control cohorts. The AUC and minimum clustering rate for fHFO in control cohort were comparable to that of the epilepsy cohort, both of which were significantly larger than sHFOs ($P < 10^{-3}$). Similar to the fHFO events of epilepsy patients, the fHFOs of control subjects did not build subclusters at low distances suggesting that their waveforms were random and non-repeating. These results indicated that fHFOs generated by the motor cortex in controls possessed similar characteristics with fHFOs of epilepsy cohort and could be differentiated from sHFOs by using the clustering ratio analysis.

Spatial correlation of high frequency oscillation waveform patterns with seizure onset zone and eloquent cortex

To explore whether the HFOs with repetitive patterns could distinguish the SOZ from functional regions, we identified stereotyped HFO waveforms within the entire HFO pool in those cases where the electrodes also covered the eloquent cortex. Based on the clustering rates given in Fig. 5B, at a radius of 0.5 we noted around 70% of sHFOs had been merged with other similar events forming subclusters, whereas 92%–95% of fHFOs remained unclustered. Consequently, we set the radius ε to 0.5 and visually inspected the spatial distribution of clustered events and those ones that had not been assigned to any subcluster using $\varepsilon = 0.5$.

Figure 6 provides representative data showing HFO distribution in those cases where the grid electrode covered SOZ and functional areas (Patients 9 and 10) or functional areas only (Patient 12 and Control 2). In the two patients where both SOZ and eloquent cortex were included, while the channels dominated by repetitive HFOs were found restricted to SOZ, the random shaped HFOs showed distinct spatial distribution suggesting a considerable portion of events located in the motor and language function areas as well as the surrounding eloquent regions. In Patient 12 and Control 2, the spatial maps of unclustered HFOs also pointed the functional motor areas identified by DCS. Overall, the results indicated that at a radius of 0.5, the percentage of unclustered HFOs that originated from outside the SOZ was significantly higher than that of the clustered HFOs (56% versus 32%, $P < 0.01$). In Patients 12 and 13, and Controls 1–5, where repetitive HFOs were rarely observed ($< 3\%$, $\varepsilon = 0.5$), the non-repetitive HFOs were concentrated around the motor cortex with the majority of them falling into the functional regions defined by DCS mapping.

Localizing the seizure onset zone using stereotyped high frequency oscillation waveforms

We observed an association between the degree of HFO signal similarity and ictogenicity, as events clustered by a smaller ε generally pinpointed those channels with higher seizure frequency. Figure 7A illustrates an example of HFO subcluster automatically identified by using different radius (0.15, 0.3 and 0.5) in Patient 9. The SOZ is represented by red dashed lines, while contact locations generating most of the seizures are marked with red solid lines. Interestingly, the spatial distribution of highly repetitive HFOs clustered by a smaller radius also reflected the epileptic brain structures generating most of the seizures.

To investigate to what extent the identification of repetitive HFOs can contribute to the accurate delineation of the SOZ, we detected the stereotypical HFOs for each patient (with SOZ definition) at varying cluster radius (similarity levels). By using the channels involving stereotyped waveforms, the sensitivity, specificity and accuracy were computed at each radius for SOZ identification. In Fig. 7B we give the results of specificity, accuracy, and the proportion of repetitive HFOs occurring inside the SOZ at each ε in Patients 1–11. Consistently in all patients, the spatial distribution of stereotyped HFOs showed agreement with clinician-defined SOZ. A specificity of 100% and an accuracy of 86% were achieved when the 'most compact' HFO subclusters were used for the SOZ prediction. In other words, all of the HFOs firstly being clustered were generated by the seizure onset regions. The averaged sensitivity was low in this case (24%, ranging from 11% to 100%),

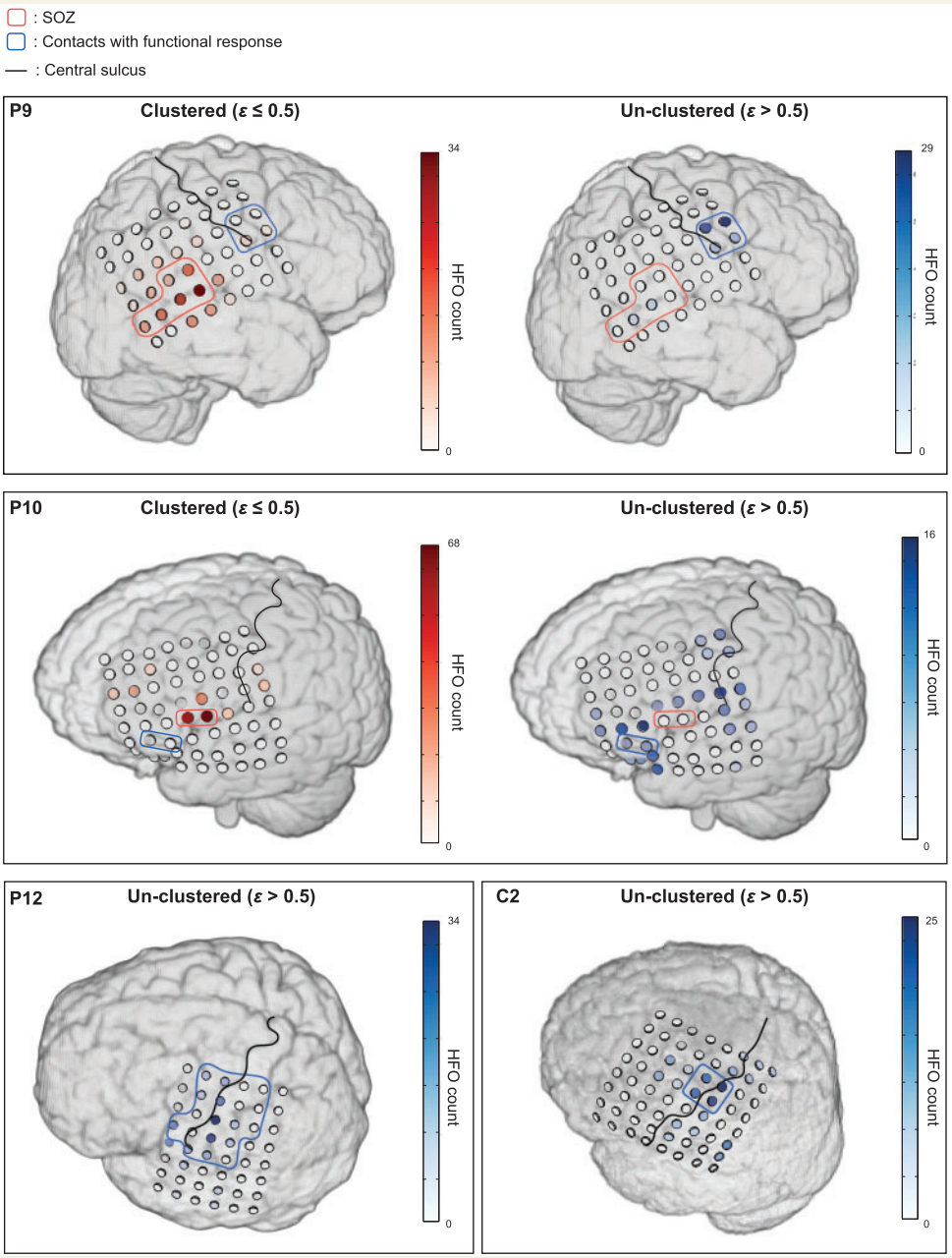

Figure 6 Spatial projection of repetitive and non-repetitive HFOs in four patients. In each patient the individual MRI together with the 3D electrode model generated directly from the co-registered CT image is shown. The 'repetitive' events are defined as the HFOs being clustered within a radius of 0.5. The results are shown for Patients 9 and 10 where both SOZ and functional cortex were covered by the grid electrodes, and for Patient 12 and Control 1 where the electrodes included the motor cortex only. Compared to the HFOs identified by using a $\varepsilon \leqslant 0.5$, the remaining unclustered HFOs are spatially localized at functional cortex or brain regions distinct from the SOZ.

as expected, because the initially identified HFO patterns consisted of a small number of events spatially concentrated to 1–5% of the total channels, making up 0.1–1% of the entire HFO pool (three to seven events per subcluster). Nevertheless, the origin of HFO subclusters with smallest diameter precisely pointed the locations responsible for the initiation of most seizures. As the cluster radius increased to 0.5, the proportion of HFOs inside the SOZ decreased by 10–87% per patient, leading to an overall specificity of 63% (20–87%), a sensitivity of 85% (38–100%) and an accuracy of 65% (25–80%). Further increase in the radius caused a significant drop in the accuracy, especially in Patient 6 where the HFOs predominantly originated from left inferior frontal region independent of the SOZ (left mesial temporal lobe), and in Patients 9–11 where the electrodes covered both the SOZ and functional regions. Using $\varepsilon = 1$, as the entire HFO pool was taken into consideration for SOZ localization, the specificity and accuracy reduced to 44% and 52%, respectively. These results suggested that the radius to detect stereotyped HFO

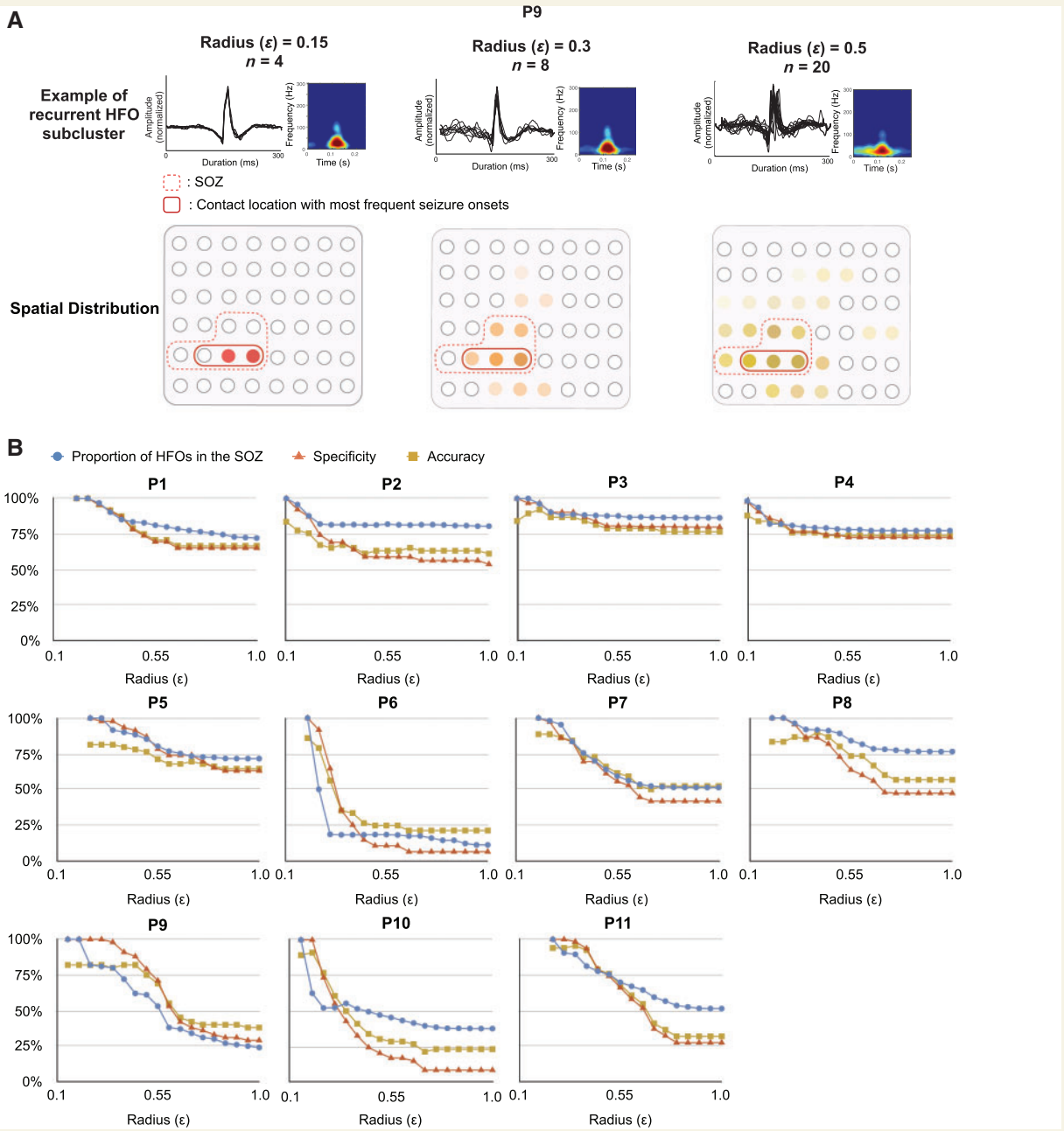

Figure 7 Spatial association of 'cloned' HFO waveforms and the SOZ. (**A**) A small radius of 0.15 identified the most stereotypical HFOs that are restricted to the contacts with the highest seizure frequency in Patient 9 (in red solid lines). As the intra-cluster similarity decreases, the clustered HFO provides a larger spatial expansion that extends beyond the SOZ. (**B**) SOZ identification performance using HFOs clustered by using radius (ε) ranging from 0.05 to 1. The specificity and percentage of HFO inside the SOZ achieve 100% in all patients when the most similar HFOs are used for SOZ localization. The numbers of identified HFOs are small, which affects the accuracy of the detection (86% on average). As the radius increases to 1, the overall specificity and accuracy decrease considerably, especially in Patients 6 and 9–11.

waveforms had to be adapted to each case for the accurate prediction of the SOZ.

In Fig. 8 we provided the spatial distribution of HFOs before executing DBSCAN (i.e. the entire HFO pool detected by Gaussian Mixture Model clustering) and the stereotypical HFO subcluster identified by minimum distance in 11 patients with clear SOZ definition. For patients who underwent successful resection surgery, we marked the channel within the resection volume to show the overlap between channels generating unclustered/clustered stereotypical HFOs and the volume of resection. In general, 60% of the HFOs before DBSCAN clustering were captured in the resection zone (10–87% per patient), whereas 100% of the repetitive HFOs clustered by minimum radius were generated from brain regions inside the resection zone, which further linked to favourable surgical outcome

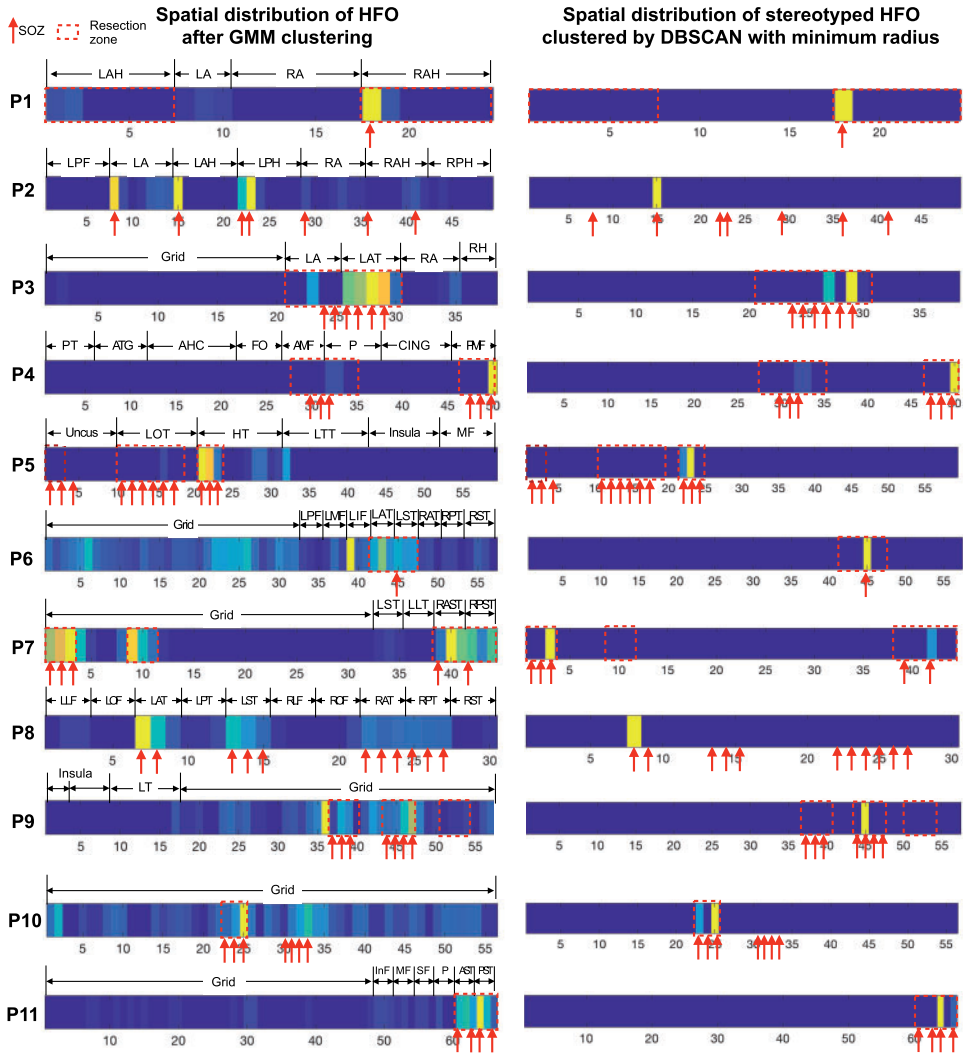

Figure 8 Spatial distribution of HFOs before (*left*) and after (*right*) DBSCAN clustering in 11 patients. The colour strips represent the HFO amount in each channel, hot colours representing the channels with a higher HFO rate. Red arrows point to the SOZ channels identified by clinicians; dashed red boxes represent the channels within the resection volume. The channels with the highest HFO rate did not always correspond to SOZ/resection zone after Gaussian Mixture Model (GMM) clustering (*left*) such as in Patients 6 and 9. For all patients, 100% of the stereotyped HFOs clustered by the minimum radius were captured in a subset of channels inside the SOZ and the resection volume (*right*). AHC = amygdala-hippocampal; ATG = anterior temporal gyrus; A/PMF = anterior/posterior middle frontal gyrus; A/PST = anterior/posterior sub-temporal; CING = cingulate; FOP = fronal operculum; HT = hippocampus tail; LOT = left occipital temporal; LTT = lateral tcans-temporal; L/RA = left/right amygdala; L/RAH = left/right anterior hippocampus; L/RAT = left/right anterior temporal; L/RLF = left/right laterial frontal; L/ROF = left/right orbital frontal; L/RPH = left/right posterior hippocampus; L/RPT = left/right posterior temporal; L/RST = left/right sub-temporal; In/M/SF = inferior/middle/superior frontal; P = parietal; PT = posterior temporal.

in these patients. In particular, capturing the stereotyped HFOs made a noticeable difference in Patients 6, 7, 9 and 10 where the electrodes covered eloquent areas or cortical regions distant from SOZ. In these patients, although many HFOs were captured in those channels out of SOZ before the subclustering of recurrent HFOs (Fig. 8, left column), we noticed that stereotyped HFOs perfectly overlapped with the SOZ and resection area (Fig. 8, right column). For each patient, the proportion of HFO subclusters inside the resection region at difference radius, ranging from 0.1–1 is also provided in Supplementary Fig. 3.

Stereotyped ripple and fast ripple oscillations

Finally, we explored the spectral content of HFOs clustered by DBSCAN in all subjects to characterize the rate of repetitive HFOs in ripple and fast ripple ranges. Supplementary Fig. 4 summarizes the proportion of stereotyped ripples versus fast ripples clustered by using radius ranging from 0.1 to 0.4. Further increase in the radius resulted in the mixing of ripple and fast ripple events and hence was not investigated. At each ε, the clustered HFO

events were visually inspected by an expert and then were assigned to 'ripple' or 'fast ripple' category based on the time-frequency maps showing their spectral peaks in the high-band. Using $\varepsilon \leqslant 0.4$, the algorithm identified 683 stereotyped fast ripples in four patients. The initial subclusters identified by the algorithm were comprised mostly of HFOs above 200 Hz, suggesting that fast ripples represented the most stereotypical HFO patterns in these patients. As the cluster radius gradually increased, the number of clustered ripples started to grow and eventually dominated the repetitive HFO category. These results indicated that compared to ripples, the presence of repetition in fast ripples was more evident in these patients, as the majority of the fast ripples formed subgroups with small radius that were identified by the algorithm at the first place.

Discussion

We found that stereotypy of automatically detected HFOs was greater at the SOZ than elsewhere in 13 patients with focal epilepsy and five control subjects without epilepsy. HFOs were simultaneously detected from inside and outside the SOZ as well as the functional regions. HFOs were first categorized into three groups based on their spatial origins. Events in the sHFO group were generated from SOZ identified by neurologists through intracranial video EEG monitoring. The other two groups, namely oHFO and fHFO, were extracted from regions outside the SOZ and from functional sites as defined by DCS, respectively. We explored the characteristics of these three groups of HFOs in terms of their traditional features, such as frequency and rate of occurrence. The results were concordant with previous studies pointing out that sHFOs had higher frequency than those detected from outside the SOZ (Matsumoto *et al.*, 2013). However, the fact that there are substantial overlaps observed across these groups supported the view that spectral frequency is not a prominent feature to determine the pathological nature of HFOs (Engel *et al.*, 2009), or to assist in the discrimination between SOZ and eloquent cortex. Mixed events recorded using micro- and macro-electrodes also suggested that epileptic HFOs might overlap with physiological HFOs in both ripple and fast ripple bands (Worrell *et al.*, 2004, 2008; Le Van Quyen *et al.*, 2010; Blanco *et al.*, 2011). Therefore, restricting the peak frequency of HFOs alone is not sufficient to assure that they are specific to SOZ.

As many of the previous studies have shown, the brain regions with a high rate of HFO activity often correlate with epileptogenesis (Bragin *et al.*, 1999; Jacobs *et al.*, 2008; Worrell *et al.*, 2008), and a complete resection of HFO-generative sites is likely to provide favourable surgical outcomes (Jacobs *et al.*, 2010; Wu *et al.*, 2010; Cho *et al.*, 2014). Nevertheless, not all HFOs were specifically linked to epileptogenicity, since they can be recorded from normal (Buzsáki and Silva, 2012) or functional areas (Staba *et al.*, 2002; Bragin *et al.*, 2007; Girardeau and Zugaro, 2011; Köhling and Staley, 2011). The fact that channels with the highest HFO rate may correspond to non-epileptic functional areas increases the complexity of HFO application in epilepsy presurgical planning. Because injury to the eloquent regions may cause irreversible neurologic impairment to the patient, it is paramount to develop methods that could efficiently and reliably identify pathological HFOs specific to the epileptogenic zones. In our data the HFO rate presented a significant difference between sHFO and oHFO groups, which was consistent with previous studies demonstrating a strong correlation between HFO rate and the SOZ (Allen *et al.*, 1992; Jirsch *et al.*, 2006; Urrestarazu *et al.*, 2006; Zijlmans *et al.*, 2011). Nonetheless, the difference in event rate between sHFO and fHFO groups showed no statistical significance, demonstrating that the rate alone may not be an accurate indicator to distinguish between SOZ and eloquent regions. It has been addressed that the use of HFOs in brain structures such as mesial temporal lobe (MTL) is limited by the inability to separate pathological HFOs from physiological activities generated over the same areas. Thus, an area with high HFO rate may not only represent an active epileptogenic region but also indicate active memory processing, which makes the current use of interictal HFOs for clinical decision premature (Jacobs *et al.*, 2012). Consequently, any process to utilize HFOs for clinical decision-making must account for this fact that there will always be a channel with the highest HFO rate, even if the recording site does not include the SOZ. Besides the spectral peak and rate of the event, other properties such as signal amplitude and duration have also been investigated in studies, but the significantly overlapped distribution highlighted the fact that the use of conventional features was not adequate to separate pathological and physiological HFOs (von Ellenrieder *et al.*, 2016). In this study we had four MTL cases. In these cases, since we could not ensure that they were associated with learning and memory functions, the HFOs, which were generated from structures out of the SOZ channels, were assigned to the oHFO group. As shown in Fig. 8, we observed that the oHFO group had irregular waveforms and most of the stereotyped HFOs were generated from the SOZ, not from the contralateral site. Our findings might be important in distinguishing between physiological and pathological HFOs in MTL epilepsy and further studies are needed to quantify the stereotyped HFO waveform patterns during controlled memory and learning tasks.

Recently, several studies suggested alternative methods to distinguish pathological HFOs by examining the interaction between high-band and low-band components of the signal. The investigators showed evidence that pathological HFOs commonly occurred before the peak of 'down' stage of slow waves (von Ellenrieder *et al.*, 2016), or modulated by activities within 3–4 Hz (Nonoda *et al.*, 2016). Yet these studies are limited by the restriction of the patients' states (rapid eye movement sleep) as well as the HFO

identification process (visual review). In the current study we detected 'clones' of HFO events by applying a density-based aggregated clustering method without presumption of any specific waveform pattern, and presented evidence that the sHFO group included small subclusters of stereotypical waveforms, whereas the fHFO waveforms were more irregular. The stereotyped patterns in sHFO were identified in all patients with SOZ regardless of the disease phenotype or implantation modalities. These results suggested that HFOs generated by epileptic tissues may present in a variety of morphological patterns such as on top of slow/sharp waves or spikes but tended to re-occur constantly throughout the recording. The oligomorphic waveform distribution of epileptic HFOs makes them distinguishable from non-epileptic HFOs, as the values of minimum radius necessary for detecting repetitive event subclusters and the areas under the clustering ratio curve in sHFO and fHFO groups showed very limited overlap. Examining the waveform patterns in the time domain enabled the separation of time series data with morphological distinctions, which might otherwise overlap in the frequency or time-frequency domains. Our results did not rule out the possibility that a random HFO pattern may still associate with the epileptic network, however it is conceivable that HFOs associated with a stereotypical pattern are more likely to be introduced by pathological circuits.

We observed that the most heterogeneous HFO patterns were seen in oHFO groups generated by cortical areas distant from the SOZ (Patients 6 and 7) or in fHFO groups where the events were detected from functional structures of epilepsy patients (Patients 9–13), as well as control subjects without seizure history (Controls 1–5). In our cases, each control subject was able to move the instructed hand or finger or responded to the stimulus in the correct way in the operating room and the detected functional areas were in accordance with anatomical landmarks and therefore these areas were accepted as normal functional regions. The inclusion of the control group provides important data regarding the spatial distribution of non-epileptic HFOs in patients without epilepsy. We noted that the clustering rate for fHFOs in the control cohort was very similar to the epilepsy cohort indicating that the nature of physiological HFOs is similar in these groups and repetitive waveforms barely originate from functional areas detected in these subjects.

By blindly detecting HFO waveforms for SOZ localization, the highly stereotyped HFO waveforms provided direct information of ictogenesis with a specificity of 100%. More importantly, we showed that the spatial origin of the most compact stereotypical HFO subclusters consistently linked to the SOZ also in difficult cases where multiple HFO generating sites were covered by electrodes, and where the HFO rate estimated from the entire pool was not a good discriminator for SOZ and other areas of the cortex. For instance, we noted that in those cases (Patients 9–11) where the electrodes covered both the SOZ and functional regions, the detection of stereotyped HFO events with the highest degree of similarity made more significant difference in the accuracy of SOZ identification compared to those cases (Patients 1–5) where the electrodes were sitting in deep brain structures and the surrounding areas.

Our observations also offered practical implications into the clinical utilization of HFOs to guide the epilepsy surgery. The unsupervised identification of repetitive HFO waveforms can be applied as a universal method without the aid of prior knowledge of any specific wave shape, which makes the approach more robust to inter-patient variation. These findings, when combined with appropriate methodologies, can provide an excellent tool for one to efficiently locate the 'core' HFOs that are highly indicative of the SOZ and separate them from eloquent cortices and other non-SOZ regions. In this context, to locate the highly stereotyped HFOs, we anticipate that one could slowly increase the radius with very fine steps until HFOs start to build the first cluster, where the corresponding channels could be used for the identification of SOZ. As an alternative strategy, an appropriate radius threshold might be estimated after executing a cross-validation procedure on a larger database. This threshold could also be adapted individually to different recording modalities obtained from depth and surface electrodes.

Our data showed that the rate and compactness of repetitive HFO waveforms are also related to the spectral content of the event. In particular, our method detected fast ripples in four patients, where we consistently observed a higher degree of waveform similarity compared to ripples, supporting the view that fast ripples might be better indicators for epileptogenesis (Bikson *et al.*, 2003; Jacobs *et al.*, 2010; Köhling and Staley, 2011). Early observations raised the hypothesis that fast ripples were distinctly pathological transients associated with the epileptic brain (Bragin *et al.*, 1999). From a cellular perspective, each pathological HFO event appears to represent co-firing of small groups of principal cells, which are pathologically interconnected (Bragin *et al.*, 2007; Foffani *et al.*, 2007). Previous studies showed evidence that ripples were associated with rhythmic firing of presumed interneurons whereas fast ripples were believed to reflect abnormal synchronous burst firing of small independent neuronal clusters of principal neurons in areas of seizure onset (Bragin *et al.*, 1999). It has been demonstrated that fast ripples are generated by the bursting activity of hyperexcitable principal cells whereas larger networks contribute to the generation of ripples other than fast ripples. We speculate that the higher rate of stereotypical waveforms with more compact structure in fast ripples could be due to involvement of small clusters of neurons and related bursting patterns. The larger networks involved in ripple generation might increase the randomness in waveform structure. Compared to fast ripples, ripples are less preferred as clinical biomarkers because they are commonly generated from a larger area including both seizure foci and non-epileptic functional brain sites (Grenier *et al.*, 2003; Engel *et al.*, 2009). It is likely that these physiological

ripples will interfere with the HFO interpretation, and most of the proposed clinical studies, particularly the ones with automatic HFO detectors applied, investigated a mixture of both physiological and pathological activities (Kerber *et al.*, 2014). It is noteworthy that in our results the highly repetitive waveforms did not exist solely in fast ripple but also in ripple oscillations. We therefore speculate that the repetition in HFO is associated with enhanced pathological synchronization in neuronal populations, and thus may reflect the underlying neuronal substrates of epileptogenesis. This finding may introduce new avenues to describe pathological and physiological HFOs other than the current spectral-based characterization.

Our analysis of the multichannel iEEG data was executed using all recorded channels in a fully automatic fashion, which differs from most of the previous studies where the investigators commonly use retrospective visual review to select HFOs from limited datasets (Worrell and Gotman, 2011). While recognizing that there is no clear demarcation between 'pathological' and 'physiological', so as the 'ripple' and 'fast ripple' HFOs, we sought to uncover the distinction between presumed HFO subclasses by utilizing unsupervised clustering technique to 'let the data speak'. It is expected that the characterization of 'cloned' signal patterns can give additional clues toward the simultaneous detection and discrimination of epileptic spikes, ripple, fast ripple, normal and pathological HFOs in human iEEG without labelling the events, which requires the existence of a yet unachievable accurate definition for different HFO subtypes. The method may benefit from the use of an extended length of recording, and need to be validated with a larger patient cohort.

Acknowledgements

We gratefully acknowledge all collaborators involved with data acquisition at Istanbul Faculty of Medicine, Texas Children's Hospital, University of Minnesota, and MD Anderson Cancer Center. We are grateful to the resources provided by TIMES. The code is available upon request.

Funding

No funding was received towards this work.

Supplementary material

Supplementary material is available at *Brain* online.

References

Alkawadri R, Gaspard N, Goncharova II, Spencer DD, Gerrard JL, Zaveri H, et al. The spatial and signal characteristics of physiologic high frequency oscillations. Epilepsia 2014; 55: 1986–95.

Allen PJ, Fish DR, Smith SJ. Very high-frequency rhythmic activity during SEEG suppression in frontal lobe epilepsy. Electroencephalogr Clin Neurophysiol 1992; 82: 155–9.

Bikson M, Fox JE, Jefferys JG. Neuronal aggregate formation underlies spatiotemporal dynamics of nonsynaptic seizure initiation. J Neurophysiol 2003; 89: 2330–3.

Blanco JA, Stead M, Krieger A, Stacey W, Maus D, Marsh E, et al. Data mining neocortical high-frequency oscillations in epilepsy and controls. Brain 2011; 134: 2948–59.

Bragin A, Engel J, Wilson CL, Fried I, Mathern GW. Hippocampal and entorhinal cortex high-frequency oscillations (100–500 Hz) in human epileptic brain and in kainic acid–treated rats with chronic seizures. Epilepsia 1999; 40: 127–37.

Bragin A, Wilson CL, Engel J. Voltage depth profiles of high-frequency oscillations after kainic acid-induced status epilepticus. Epilepsia 2007; 48 (Suppl 5): 35–40.

Brna P, Duchowny M, Resnick T, Dunoyer C, Bhatia S, Jayakar P. The diagnostic utility of intracranial EEG monitoring for epilepsy surgery in children. Epilepsia 2015; 56: 1065–70.

Burnos S, Frauscher B, Zelmann R, Haegelen C, Sarnthein J, Gotman J. The morphology of high frequency oscillations (HFO) does not improve delineating the epileptogenic zone. Clin Neurophysiol 2016; 127: 2140–8.

Burnos S, Hilfiker P, Sürücü O, Scholkmann F, Krayenbühl N, Grunwald T, et al. Human intracranial high frequency oscillations (HFOs) detected by automatic time-frequency analysis. PLoS One 2014; 9: e94381.

Buzsáki G, Silva FL. High frequency oscillations in the intact brain. Prog Neurobiol 2012; 98: 241–9.

Cho JR, Koo DL, Joo EY, Seo DW, Hong SC, Jiruska P, et al. Resection of individually identified high-rate high-frequency oscillations region is associated with favorable outcome in neocortical epilepsy. Epilepsia 2014; 55: 1872–83.

de Tisi J, Bell GS, Peacock JL, McEvoy AW, Harkness WF, Sander JW, et al. The long-term outcome of adult epilepsy surgery, patterns of seizure remission, and relapse: a cohort study. Lancet 2011; 378: 1388–95.

Dümpelmann M, Jacobs J, Kerber K, Schulze-Bonhage A. Automatic 80-250Hz 'ripple' high frequency oscillation detection in invasive subdural grid and strip recordings in epilepsy by a radial basis function neural network. Clin Neurophysiol 2012; 123: 1721–31.

Engel J. Surgical treatment of the epilepsies. New York, NY: Raven Press; 1987.

Engel J Jr, Bragin A, Staba R, Mody I. High-frequency oscillations: what is normal and what is not? Epilepsia 2009; 50: 598–604.

Engel J Jr, Henry TR, Risinger MW, Mazziotta J, Sutherling W, Levesque MF, et al. Presurgical evaluation for partial epilepsy: relative contributions of chronic depth-electrode recordings versus FDG-PET and scalp-sphenoidal ictal EEG. Neurology 1990; 40: 1670–7.

Engel J Jr, Wiebe S, French J, et al. Practice parameter: temporal lobe and localized neocortical resections for epilepsy. Neurology 2003; 60: 538–47.

Ester M, Kriegel HP, Sander J, Xu X. A density-based algorithm for discovering clusters in large spatial databases with noise [Internet]. In: Proceedings of the Second International Conference on Knowledge Discovery and Data Mining. 1996. p. 226–31.

Foffani G, Uzcategui YG, Gal B, Menendez de la Prida L. Reduced spike-timing reliability correlates with the emergence of fast ripples in the rat epileptic hippocampus. Neuron 2007; 55: 930–41.

Girardeau G, Zugaro M. Hippocampal ripples and memory consolidation. Curr Opin Neurobiol 2011; 21: 452–9.

Grenier F, Timofeev I, Steriade M. Neocortical very fast oscillations (ripples, 80-200 Hz) during seizures: intracellular correlates. J Neurophysiol 2003; 89: 841–52.

Henry TR, Ross DA, Schuh LA, Drury I. Indications and outcome of ictal recording with intracerebral and subdural electrodes in

refractory complex partial seizures. J Clin Neurophysiol 1999; 16: 426–38.
Jacobs J, LeVan P, Chander R, Hall J, Dubeau F, Gotman J. Interictal high-frequency oscillations (80-500 Hz) are an indicator of seizure onset areas independent of spikes in the human epileptic brain. Epilepsia 2008; 49: 1893–907.
Jacobs J, Staba R, Asano E, Otsubo H, Wu JY, Zijlmans M, et al. High-frequency oscillations (HFOs) in clinical epilepsy. Prog Neurobiol 2012; 98: 302–15.
Jacobs J, Zijlmans M, Zelmann R, Chatillon CE, Hall J, Olivier A, et al. High-frequency electroencephalographic oscillations correlate with outcome of epilepsy surgery. Ann Neurol 2010; 67: 209–20.
Jirsch JD, Urrestarazu E, LeVan P, Olivier A, Dubeau F, Gotman J. High-frequency oscillations during human focal seizures. Brain 2006; 129: 1593–608.
Katariwala NM, Bakay RA, Pennell PB, Olson LD, Henry TR, Epstein CM. Prolonged remission of intractable partial epilepsy following implantation of intracranial electrodes. Neurology 2001; 57: 1505–8.
Kaufman L, Rousseeuw PJ. Clustering by means of medoids. In: Dodge Y, editor. Statistical Data Analysis Based on the L1-Norm and Related Methods. Switzerland: Springer-Verlag New York; 2002. p. 405–16.
Kerber K, Dümpelmann M, Schelter B, Le Van P, Korinthenberg R, Schulze-Bonhage A, et al. Differentiation of specific ripple patterns helps to identify epileptogenic areas for surgical procedures. Clin Neurophysiol 2014; 125: 1339–45.
Ketchen D, Shook C. The application of cluster analysis in strategic management research: an analysis and critique. Strateg Manage J 1996; 17: 441–58.
Köhling R, Staley K. Network mechanisms for fast ripple activity in epileptic tissue. Epilepsy Res 2011; 97: 318–23.
Kucewicz MT, Cimbalnik J, Matsumoto JY, Brinkmann BH, Bower MR, Vasoli V, et al. High frequency oscillations are associated with cognitive processing in human recognition memory. Brain 2014; 137: 2231–44.
Le Van Quyen M, Staba R, Bragin A, Dickson C, Valderrama M, Fried I, et al. Large-scale microelectrode recordings of high-frequency gamma oscillations in human cortex during sleep. J Neurosci 2010; 30: 7770–82.
Liu S, Ince NF, Abosch A, Henry TR, Sha Z. Investigation of automatically detected high frequency oscillations (HFOs) as an early predictor of seizure onset zone. Conf Proc IEEE Eng Med Biol Soc 2015; 2015: 6602–5.
Liu S, Sha Z, Sencer A, Aydoseli A, Bebek N, Abosch A, et al. Exploring the time-frequency content of high frequency oscillations for automated identification of seizure onset zone in epilepsy [Internet]. J Neural Eng 2016; 13: 026026. Available from: http://www.ncbi.nlm.nih.gov/pubmed/26924828
Matsumoto A, Brinkmann BH, Matthew Stead S, Matsumoto J, Kucewicz MT, Marsh WR, et al. Pathological and physiological high-frequency oscillations in focal human epilepsy. J Neurophysiol 2013; 110: 1958–64.
Melani F, Zelmann R, Mari F, Gotman J. Continuous high frequency activity: a peculiar SEEG pattern related to specific brain regions. Clin Neurophysiol 2013; 124: 1507–16.
Nagasawa T, Juhász C, Rothermel R, Hoechstetter K, Sood S, Asano E. Spontaneous and visually driven high-frequency oscillations in the occipital cortex: intracranial recording in epileptic patients. Hum Brain Mapp 2012; 33: 569–83.
Nonoda Y, Miyakoshi M, Ojeda A, Makeig S, Juhász C, Sood S, et al. Interictal high-frequency oscillations generated by seizure onset and eloquent areas may be differentially coupled with different slow waves. Clin Neurophysiol 2016; 127: 2489–99.
Sinai A, Bowers CW, Crainiceanu CM, Boatman D, Gordon B, Lesser RP, et al. Electrocorticographic high gamma activity versus electrical cortical stimulation mapping of naming. Brain 2005; 128: 1556–70.
So N, Gloor P, Quesney LF, Jones-Gotman M, Olivier A, Andermann F. Depth electrode investigations in patients with bitemporal epileptiform abnormalities. Ann Neurol 1989; 25: 423–31.
Staba RJ, Wilson CL, Bragin A, Fried I, Engel J. Quantitative analysis of high-frequency oscillations (80-500 Hz) recorded in human epileptic hippocampus and entorhinal cortex. J Neurophysiol 2002; 88: 1743–52.
Traub RD, Whittington MA, Buhl EH, LeBeau FE, Bibbig A, Boyd S, et al. A possible role for gap junctions in generation of very fast EEG oscillations preceding the onset of, and perhaps initiating, seizures. Epilepsia 2001; 42: 153–70.
Urrestarazu E, Jirsch JD, LeVan P, Hall J. High-frequency intracerebral EEG activity (100–500 Hz) following interictal spikes. Epilepsia 2006; 47: 1465–76.
von Ellenrieder N, Frauscher B, Dubeau F, Gotman J. Interaction with slow waves during sleep improves discrimination of physiologic and pathologic high-frequency oscillations (80-500 Hz). Epilepsia 2016; 57: 869–78.
Worrell G, Gotman J. High-frequency oscillations and other electrophysiological biomarkers of epilepsy: clinical studies. Biomark Med 2011; 5: 557–66.
Worrell GA, Gardner AB, Stead SM, Hu S, Goerss S, Cascino GJ, et al. High-frequency oscillations in human temporal lobe: simultaneous microwire and clinical macroelectrode recordings. Brain 2008; 131: 928–37.
Worrell GA, Parish L, Cranstoun SD, Jonas R, Baltuch G, Litt B. High-frequency oscillations and seizure generation in neocortical epilepsy. Brain 2004; 127: 1496–506.
Wu JY, Sankar R, Lerner JT, Matsumoto JH, Vinters HV, Mathern GW. Removing interictal fast ripples on electrocorticography linked with seizure freedom in children. Neurology 2010; 75: 1686–94.
Zijlmans M, Jacobs J, Kahn YU, Zelmann R, Dubeau F, Gotman J. Ictal and interictal high frequency oscillations in patients with focal epilepsy. Clin Neurophysiol 2011; 122: 664–71.
Zijlmans M, Jiruska P, Zelmann R, Leijten FS, Jefferys JG, Gotman J. High-frequency oscillations as a new biomarker in epilepsy. Ann Neurol 2012; 71: 169–78.